Optimal Placement of Landmarks for Indoor Localization using Sensors with a Limited Range

Payam Nazemzadeh[1]

[1]Dep. of Information Engineering and Computer Science
University of Trento, Trento, Italy
E–mail: payam.nazemzadeh@unitn.it

Daniele Fontanelli[2], David Macii[2]

[2]Dep. of Industrial Engineering
University of Trento, Trento, Italy
E–mail: {daniele.fontanelli,david.macii}@unitn.it

Abstract—Indoor positioning often requires detecting and recognizing ad-hoc landmarks or anchor points with known coordinates and/or a given orientation within a given reference frame. Typically, the available kind of sensors and their detection area determine the landmark features and position. Of course, an excessive use of landmarks pose serious scalability and cost issues, whereas, on the other hand, a too-low amount of deployed landmarks may create areas where agent's position is hard to track or localization accuracy drops. In addition, often sensors are not omni-directional. In this paper, the optimal placement problem of landmarks detected by sensors with a limited detection area is addressed in the general case of wide-open, ideally unbounded, rooms. First, landmarks placement optimization is performed numerically. Then, a closed-form expression of the optimal distance between landmarks on a regular pattern is determined as a function of both the reading range and the directional properties of the sensor considered. Finally, the performances of the chosen placement strategy in more realistic indoor environments (i.e. consisting of multiple rooms with obstacles therein) are evaluated through simulations assuming, without loss of generality, that a wheeled robot equipped with a front camera adjusts its own position by detecting suitable visual landmarks.

Keywords—*Indoor localization, position tracking, landmark placement, optimization, frameworks for hybrid positioning, performance evaluation.*

I. INTRODUCTION

Indoor localization has increasingly gained importance in a large variety of applications, such as logistics, customers assistance in public places, industrial robotics and ambient assisted living (AAL) services. Although infrastructure-free indoor localization is ideally cheaper and more flexible, it is usually still not accurate enough when performance requirements are demanding. Various indoor localization solutions have been proposed over the last few years, e.g. based on time-of-flight (ToF) and/or radio signal strength intensity (RSSI) measurements [1], [2], detection of radio frequency identification (RFID) tags [3], [4], ultrasonic sonars [5], and optical or vision-based systems [6].

In spite of the significant differences between such sensing technologies, a common feature to all of them is the need for deploying appropriate reference devices in the environment where possible targets are supposed to be localized and tracked. Usually, such devices (sometimes referred to as "anchor nodes", "tags", "markers" or "landmarks", depending on whether they are active or passive and on the kind of sensing technology adopted) have known coordinates and/or orientation in a given reference frame. In the rest of this paper, without loss of generality, it will be assumed that the landmarks are readable by means of sensors (e.g. cameras or RFID readers) installed on the agent to be localized. In principle, these sensors can also measure the relative position and orientation between the agent and a detected landmark. While these relative measurements can definitely improve positioning accuracy, they are not strictly needed for the purposes of this paper, which is focused just on where landmarks should be placed, regardless of how they are actually used by a specific localization system. Therefore, the analysis described in this paper is absolutely general. Of course, the number landmarks in the environment should be as small as possible, while still providing reliable and accurate localization.

Depending on the application and on the chosen sensing technology, landmarks can be detected continuously or intermittently. In the former case, the optimal landmark placement is the one for which, ideally, just one landmark is detected at every sampling time. In the latter case, the number of landmarks can be much smaller, thus reducing deployment complexity and costs. In principle, a localization system should be also able to track the agent's position even when no landmarks are detected [7]. Of course, the landmark placement problem strongly depends on the detection area of the sensor in use. In [8] a strip of RFID tags is deployed in such a way that, in every position, at least one RFID tag lies within the detection range of the on-board reader. The strip has an equilateral triangular shape, with the RFID tags being located in the vertices. In [9] authors show that, in the case of landmark patterns consisting of equilateral triangles, the maximum side length is $\sqrt{3}$ times larger than the detection range. However, other kinds of patterns are also possible, and they can be composed by up to 8-sided polygons [10]. A complete discussion about the landmark placement over rectangular patterns in the case of sensors with an omni-directional reading range is presented in [11]. Beinhofer et al. [12] solved the NP-hard sensor placement problem analytically assuming to have predefined robot trajectories. Using observability constraints, such a deployment strategy has been modified in order to be robust to missed landmarks, e.g. because of dynamic obstacles or failures [13]. The main drawback of this solution is the constraint imposed by the limited number of specific trajectories.

Some optimal landmark placement strategies have obtained by solving the so-called "art gallery problem". In this case,

the area of a given environment (i.e. the art gallery) has to be partitioned into regions, in order to minimize the number of "guards" (i.e. the landmarks in this case) that can view every point of each region. This analysis allows to select the landmarks position ensuring that at every location at least one landmark can be detected [14]. The simulated annealing technique is frequently used to solve this kind of problems [15]. Unfortunately, the placement strategies based on the "art gallery problem" are effective when the landmarks are supposed to be active. This fact poses additional deployment problems, since each landmark has to be properly powered. Moreover, landmark detection depends not only on the distance between the sensor and one landmark, but also on their relative orientation. This happens, for instance, when well-known low-cost systems, such as simple cameras or ultrasonic sensors, are employed. However, a similar scenario holds also when wireless systems with strongly directional antennas are used.

The goal of this paper is to find a general solution to the landmark placement problem, when the sensor detection area (SDA) has a limited angular range and the agent's motion is not constrained. Assuming to represent the SDA (e.g. the field of view of a standard RGB-D camera) with a polytope, first an optimal solution based on numerical techniques is introduced and discussed. Then, it will be shown that similar results can be achieved analytically. The proposed approach guarantees the detection of at least one landmark at every sampling time, regardless of agent's trajectory and sensor orientation, provided that the agent moves in a wide-open, ideally unbounded, room. In real environments landmark detection cannot be always guaranteed because of static and dynamic obstacles. Nonetheless, the probability of landmark detection can be kept sufficiently large and, more importantly, the localization uncertainty can be kept bounded, thus paving the way to further optimization strategies if intermittent landmark observations can be tolerated.

The rest of the paper is organized as follows. In Section II the optimal placement problem is formulated and both numerical and analytical solutions are derived. The results of some simulations confirming the correctness of such solutions are reported in Section III. Further Monte Carlo simulation results in both wide-open unbounded rooms and in a realistic environment (i.e. the premises of the Department of Information Engineering and Computer Science of the University of Trento) are shown in Section IV to evaluate the performances of optimal placement in a case study, i.e. when a wheeled robot equipped with a front camera adjusts its own position using visual landmarks. Finally, Section V concludes the paper and presents future applications of the proposed solution.

II. Optimal Landmarks Placement

As briefly explained in the Introduction, the purpose of this paper is to determine the minimum number of landmarks to be deployed in a given environment so that, for any given configuration of the sensing system, at least one landmark lies within the SDA. This problem is often treated in the literature as a *tiling* problem, where the vertices of the tiles coincide with landmarks' positions. It is known that only three periodic, monohedral and regular tiling patterns exist in $\mathbb{R}^2$ (namely over the plane), i.e. triangles, squares and hexagons [16], [17]. Using triangle and square tiles (which are the easiest to deploy
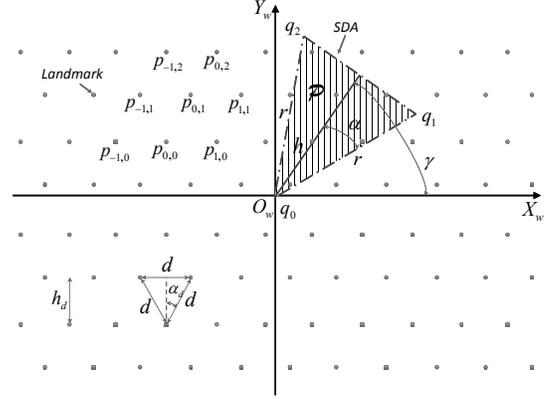

Fig. 1. Points of an A^2 lattice representing the possible landmark positions in a wide-open, unbounded room. The sensor detection area (SDA) is represented by the shadowed region inside polytope $\mathcal{P}$.

in practice) the vertices of all polytopes belong to an A^2 *point lattice* and a *square point lattice*, respectively. Thus, if the polytope $\mathcal{P}$ represents the SDA, the original optimization problem can be regarded as *"the problem of finding whether the polytope contains a lattice point"* for any possible position and orientation of $\mathcal{P}$ [17]. Limiting the analysis to the case of triangular tiles only (the extension to the square case is similar and is left for future work), a convenient way to represent the lattice points on a plane is to assume that one of the triangle sides is parallel to the X_w axis of the reference frame $\langle W \rangle = \{O_w, X_w, Y_w\}$, as shown in Fig. 1. If $p_{0,0} = [x_0, y_0]^T$ denotes a given lattice reference point, the coordinates of any other point of the lattice can be expressed as

$$p_{i,j} = p_{0,0} + \begin{bmatrix} j\frac{d}{2} + id \\ jh_d \end{bmatrix}, \quad \forall i, j \in \mathbb{Z}, \qquad (1)$$

where d, $\alpha_d = \pi/6$ and $h_d = d\cos(\alpha_d)$ are the side length, the semi-angle and the height of any equilateral triangle, respectively. Observe that d is also the distance between every pair of adjacent landmarks. For the sake of simplicity, but without loss of generality, in this paper the polytope $\mathcal{P}$ defining the SDA is approximated with an isosceles triangle with a vertex angle of 2α, $\alpha \in (0, \pi/2)$ and height h (see Figure 1). Thus, the two equal sides of the triangular SDA have length $r = h/\cos(\alpha)$. Moreover, if γ denotes the orientation angle of the SDA with respect to axis X_w, the polytope is defined as the plane portion

$$\mathcal{P} \triangleq \left\{ \sum_{i=0}^{2} \lambda_i q_i \, \Big| \, \sum_{i=0}^{2} \lambda_i = 1, \lambda_i \in [0, 1] \text{ for } i = 0, 1, 2 \right\}, \quad (2)$$

where $q_0 = O_w = [0, 0]^T$,

$$q_1 = r \begin{bmatrix} \sin(\beta + \gamma) \\ -\cos(\beta + \gamma) \end{bmatrix}, \qquad q_2 = r \begin{bmatrix} \sin(\beta - \gamma) \\ \cos(\beta - \gamma) \end{bmatrix}, \quad (3)$$

are the SDA vertices and $\beta = \pi/2 - \alpha$ is the angle between segment $\overline{q_0 q_1}$ and axis X_w when $\gamma = \pi/2$, as shown in Fig. 1.

Notice that, due to the symmetry and periodicity of the triangular lattice, in order to generate all the possible lattice positions, it is sufficient to move the reference point $p_{0,0}$ in
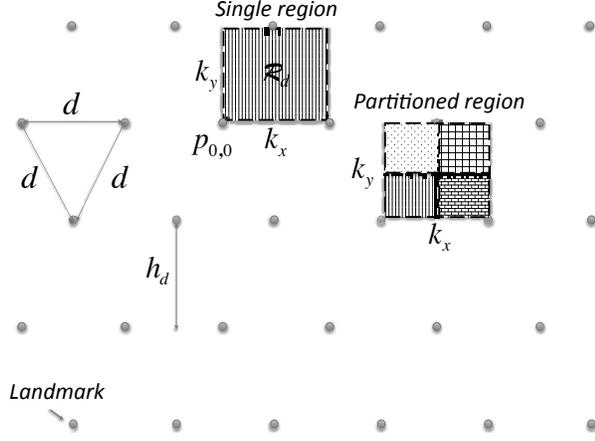
Fig. 2. Possible landmark positions in the rectangle $\mathcal{R}_d$ and corresponding partitions.

the rectangle $\mathcal{R}_d$ with base d and height h_d, as pictorially explained in Fig. 2. Therefore, with reference to the notation introduced above, the optimal landmarks placement problem can be formulated as follows, i.e.

Problem 1: Maximize the landmark distance d such that $\forall p_{0,0} \in \mathcal{R}_d$ and $\forall \gamma \in [0, 2\pi)$ there exists at least one $p_{i,j} \in \mathcal{P}$ with $i, j \in \mathbb{Z}$.

In the following subsections, first a numerical solution to solve this problem is presented. Then, a closed-form analytical solution is also derived.

A. Optimal numerical solution

According to Problem 1, a solution should be found $\forall p_{0,0} \in \mathcal{R}_d$. Hence, we can rewrite

$$p_{0,0} = \begin{bmatrix} x_0 \\ y_0 \end{bmatrix} + \begin{bmatrix} k_x d \\ k_y h_d \end{bmatrix} = \begin{bmatrix} x_0 \\ y_0 \end{bmatrix} + \begin{bmatrix} k_x d \\ k_y d c_6 \end{bmatrix},$$

where $c_6 = \cos(\pi/6)$ and $k_x, k_y \in [0, 1]$. The area of $\mathcal{R}_d$ as a *single region* is shadowed in Fig. 2. Given that $[x_0, y_0]^T$ is generic, we can choose $[x_0, y_0]^T = [0, 0]^T$ for simplicity. As a consequence, it follows from (1) that

$$p_{i,j} = \begin{bmatrix} k_x d + j\frac{d}{2} + id \\ k_y d c_6 + j d c_6 \end{bmatrix} = d \begin{bmatrix} \frac{1}{2}(2k_x + j + 2i) \\ c_6(k_y + j) \end{bmatrix}. \quad (4)$$

According to the definition of polytope (2), a point $p_{i,j} \in \mathcal{P}$ if and only if $\exists \lambda_1, \lambda_2 \in [0, 1]$ such that $\lambda_1 q_1 + \lambda_2 q_2 = p_{i,j}$, with $\lambda_1 + \lambda_2 \leq 1$. Recalling (3), if we define

$$Q_\gamma = [q_1, q_2] = r \begin{bmatrix} \sin(\beta + \gamma) & \sin(\beta - \gamma) \\ -\cos(\beta + \gamma) & \cos(\beta - \gamma) \end{bmatrix}, \quad (5)$$

and $\Lambda = [\lambda_1, \lambda_2]^T$, it follows that

$$Q_\gamma \Lambda = p_{i,j} \Rightarrow \Lambda = Q_\gamma^{-1} p_{i,j}, \quad (6)$$

where the inverse of Q_γ always exists since $\det(Q_\gamma) = r \sin(2\beta) \neq 0$, being r and β larger than 0. Once the Λ values given by (6) and expressed as a function of the elements of (4)

are compared with the related constraints, it is shown in the Appendix that the following system of inequalities results

$$\begin{cases} \dfrac{\cos(\beta - \gamma)}{2}(2k_x + j + 2i) - \sin(\beta - \gamma)c_6(k_y + j) \geq 0, \\ \dfrac{\cos(\beta + \gamma)}{2}(2k_x + j + 2i) + \sin(\beta + \gamma)c_6(k_y + j) \geq 0, \quad (7) \\ d \left[\dfrac{\cos(\gamma)}{2}(2k_x + j + 2i) + \sin(\gamma)c_6(k_y + j) \right] \leq h. \end{cases}$$

Therefore, a point $p_{i,j} \in \mathcal{P}$ if and only if $\exists i, j \in \mathbb{Z}$ satisfying (7). Therefore, to solve Problem 1, we have to find a solution to system (7) for any possible value of variables γ, k_x and k_y. Notice that:

1) All the inequalities of (7) are linear in $i, j \in \mathbb{Z}$ for given values of γ, k_x and k_y.
2) Since the coefficients of (7) depend on periodic trigonometric functions, just the values of γ in the interval $[0, \pi/2]$ should be taken into consideration. This is a direct consequence of the regular, periodic structure of the lattice. While the possible values of γ are infinite, being the range of variation limited and $i, j \in \mathbb{Z}$, in practice just a finite amount of γ values (e.g. chosen with a resolution of $\pi/40$) can be explored to find the optimal solution.
3) Given that the objective of Problem 1 is to maximize d, the first two inequalities in (7) provide the constraints to the possible values of $i, j \in \mathbb{Z}$, whereas the third inequality represents the actual cost function to optimize. By adding the first two inequalities and by using basic trigonometric functions properties, it can be easily proved that $\frac{\cos(\gamma)}{2}(2k_x + j + 2i) + \sin(\gamma)c_6(k_y + j) > 0$. Therefore, since $\cos(\gamma) \geq 0$, $\sin(\gamma) \geq 0$ and $k_x, k_y \in [0, 1]$, it ensues immediately that the maximum of d for a given γ (denoted as d_γ in the following) is obtained for those value of $i, j \in \mathbb{Z}$ minimizing the cost function $f_\gamma J$, where

$$f_\gamma = \begin{bmatrix} \cos(\gamma) & \frac{\cos(\gamma)}{2} + \sin(\gamma)c_6 \end{bmatrix}, \quad (8)$$

and $J = [i, j]^T$.

In light of the previous remarks, we can rewrite the first two linear inequalities of (7) in a compact, matrix form, i.e. $A_1 J \geq B_1 K_1$ and $A_2 J \geq B_2 K_2$, respectively, where

$$A_1 = \begin{bmatrix} \cos(\beta - \gamma) & \frac{\cos(\beta - \gamma)}{2} - \sin(\beta - \gamma)c_6 \end{bmatrix}$$

$$A_2 = \begin{bmatrix} \cos(\beta + \gamma) & \frac{\cos(\beta + \gamma)}{2} + \sin(\beta + \gamma)c_6 \end{bmatrix},$$

$$B_1 = \begin{bmatrix} -\cos(\beta - \gamma) & \sin(\beta - \gamma)c_6 \end{bmatrix},$$

$$B_2 = \begin{bmatrix} -\cos(\beta + \gamma) & -\sin(\beta + \gamma)c_6 \end{bmatrix}$$

Note that if $K = [k_x, k_y]^T$ denotes a vector of generic coefficients, $K_1 = [k_{x_1}, k_{y_1}]^T$ and $K_2 = [k_{x_2}, k_{y_2}]^T$ are the specific values that, in the worst case, maximize $B_1 K$ and $B_2 K$, respectively. Therefore, for a given $\gamma \in [0, \pi/2]$, the solution $i^\star, j^\star \in \mathbb{Z}$ of the following optimal problem

$$\begin{aligned} \min_{i,j} \quad & f_\gamma J \\ \text{s.t.} \quad & A_1 J \geq B_1 K_1, \\ & A_2 J \geq B_2 K_2, \quad (9) \\ & i, j \in \mathbb{Z}, \end{aligned}$$
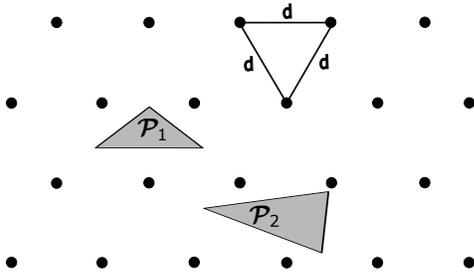
Fig. 3. Pictorial examples of missed landmark detection, when the geometrical constraints $d \leq r$ (e.g. $\mathcal{P}_1$) and $d \leq b$ (e.g. $\mathcal{P}_2$) are not satisfied.

can be used to compute the maximum distance d_γ for a given γ, i.e.

$$d_\gamma = \frac{2h}{\cos(\gamma)(2k_x + j^\star + 2i^\star) + 2\sin(\gamma)c_6(k_y + j^\star)}. \quad (10)$$

It is worthwhile to note that a solution to Problem (9) always exists since $\det([A_1^T, A_2^T]^T) = \sin(2\beta)c_6 \neq 0$. Also, $p_{i^\star,j^\star} \in \mathcal{P}$, $\forall k_x, k_y \in [0,1]$, determines a single point that belongs to the SDA $\forall p_{0,0} \in \mathcal{R}_d$. This is clearly an overkill, since it is sufficient that at least *one* point belongs to the SDA, even if this is not *the same* point $\forall k_x, k_y \in [0,1]$. To address this issue, $\mathcal{R}_d$ can be partitioned into smaller sub-regions (i.e. by bisecting k_x and k_y iteratively) in order to compute the optimal pair $i^\star, j^\star \in \mathbb{Z}$ for each sub-region (see the *Partitioned region* in Fig. 2 for reference). Therefore, if $\mathcal{J}^\star$ denotes the set of optimal $i^\star$, $j^\star$ pairs of all sub-regions, the optimal distance between landmarks for a given γ results from

$$d_\gamma^\star = \min_{i^\star, j^\star \in \mathcal{J}^\star} \frac{2h}{\cos(\gamma)(2k_x + j^\star + 2i^\star) + 2\sin(\gamma)c_6(k_y + j^\star)}. \quad (11)$$

Finally, the optimal solution to Problem 1 is given by

$$d^\star = \min_{\gamma \in [0, \pi/2]} d_\gamma^\star. \quad (12)$$

The results of some simulations confirming the validity of the proposed optimal solution are reported in Section III.

B. Optimal analytical solution

This Section provides an analytical expression of the optimal distance between landmarks, when an A^2 lattice in a wide-open unbounded room is considered. Let $b = 2r\sin(\alpha)$ be the SDA maximum width, i.e. the length of the base of the isosceles triangle $\mathcal{P}$. In order to solve Problem 1, two geometrical constraints must be satisfied, i.e. $d \leq r$ and $d \leq b$. Indeed, if these constraints are not met, at least one triple of values k_x, k_y and γ exists such that the sensor cannot detect any landmark (e.g. $\mathcal{P}_1$ and $\mathcal{P}_2$ in Fig. 3). Let us consider a *virtual* sensor with a triangular SDA included into $\mathcal{P}$. Similarly to (2), the SDA of the virtual sensor is defined as follows, i.e.

$$\mathcal{P}^v \triangleq \left\{ \sum_{i=0}^{2} \lambda_i q_i^v \mid \sum_{i=0}^{2} \lambda_i = 1, \lambda_i \in [0,1] \text{ for } i = 0, 1, 2 \right\}, \quad (13)$$

where $q_0^v = q_0$ and

$$q_1^v = r^v \begin{bmatrix} \sin(\beta + \gamma) \\ -\cos(\beta + \gamma) \end{bmatrix}, q_2^v = r^v \begin{bmatrix} \sin(\beta - \gamma) \\ \cos(\beta - \gamma) \end{bmatrix},$$
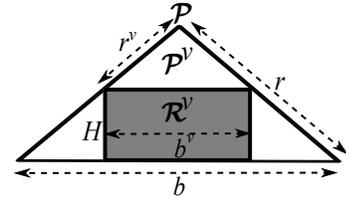

Fig. 4. The rectangle $\mathcal{R}^v$ in front of the FoV $\mathcal{P}^v$.

with $r^v \leq r$, $d \leq r^v$ and $d \leq b^v = 2r^v \sin(\alpha)$, in accordance with the constraints specified above. Let $\mathcal{R}^v$ be the rectangle, with base b^v and height $H = h - h^v = (r - r^v)\cos(\alpha)$, which lies just beyond the SDA of the virtual sensor (see Figure 4 for reference). Observe that, in general, $\{\mathcal{P}^v \cup \mathcal{R}^v\} \subseteq \mathcal{P}$. So $\{\mathcal{P}^v \cup \mathcal{R}^v\}$ can be regarded as an inner approximation of polytope $\mathcal{P}$, which becomes increasingly accurate as $r^v \to r$. In light of this approximation, a sub-optimal version of Problem 1 can be formulated as follows, i.e.

Problem 2: Maximize the landmark distance d such that $\forall p_{0,0} \in \mathcal{R}_d$ and $\forall \gamma \in [0, 2\pi)$ there exists at least one pair $i, j \in \mathbb{Z}$ with $p_{i,j} \in \{\mathcal{P}^v \cup \mathcal{R}^v\}$.

To find an analytical solution to this problem, first of all notice that $\max d = \min(r, b^v)$, as $b_v \leq b$. Given that α, b and r are known parameters of the sensor, but b^v is unknown, using simple geometric arguments, it can be shown that

$$b^v = 2\tan(\alpha)(r\cos(\alpha) - H). \quad (14)$$

Therefore, in order to maximize b^v it is sufficient to minimize H. Let us suppose that, for a given choice of k_x, k_y and γ, then $p_{i,j} \notin \mathcal{P}^v$ for any $i, j \in \mathbb{Z}$ (otherwise Problem 2 would be straightforwardly solved). Under this assumption, we need to have one landmark in $\mathcal{R}^v$. This in turn implies that $\mathcal{R}_d \subseteq \mathcal{R}^v$, where the areas of $\mathcal{R}_d$ and $\mathcal{R}^v$ are equal to $d \cdot h_d$ and $H \cdot b^v$, respectively. Since $d \leq b^v$, the minimum value of H ensuring that $\mathcal{R}_d \subseteq \mathcal{R}^v$ is

$$H = h_d = d\frac{\sqrt{3}}{2}. \quad (15)$$

Thus, by plugging (15) into (14), it finally results that

$$d \leq d^\dagger = b^v = r\frac{2\sin(\alpha)}{1 + \sqrt{3}\tan(\alpha)}. \quad (16)$$

where $d^\dagger$ denotes the analytical solution to Problem 2. Notice that $0 < d^\dagger < r$, because $\alpha \in (0, \pi/2)$.

III. SIMULATION-BASED VALIDATION OF NUMERICAL AND ANALYTICAL OPTIMAL SOLUTIONS

In order to confirm that the optimal landmark distances obtained both numerically and analytically are correct and converge to the same solution, some meaningful simulations have been performed. Fig. 5 shows the optimal landmark distances normalized by r (i.e. $\frac{d^\star}{r}$ and $\frac{d^\dagger}{r}$) as a function of the sensor angular semi-range $\alpha \in (0, \pi/2)$. In the numerical case, three sets of results are reported for different partitions of $\mathcal{R}_d$ (i.e. assuming to find a solution in the entire $\mathcal{R}_d$, in 8 sub-regions and in 64 sub-regions of $\mathcal{R}_d$, respectively). Notice that as the number of partitions used to compute $d^\star$ grows, the sub-optimal numerical values exhibit smaller fluctuations (due to the finer granularity of the regions explored) and
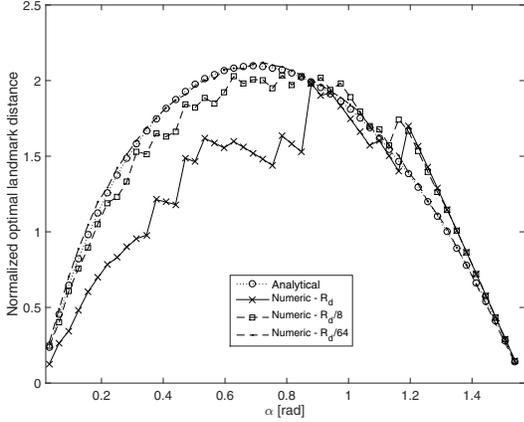
Fig. 5. Optimal landmark distances (normalized by r) computed numerically and analytically as a function of the sensor angular semi-range α. The numerical results refer to three different partitions of $\mathcal{R}_d$.
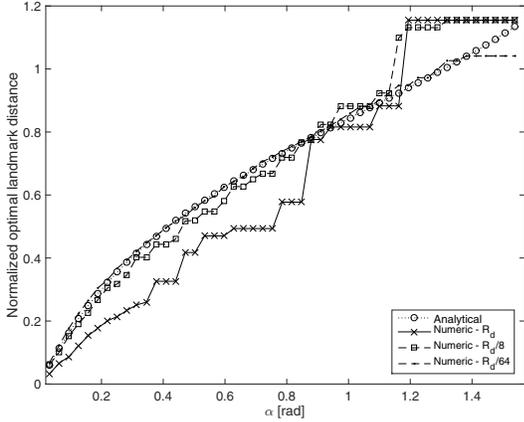

Fig. 6. Optimal landmark distances (normalized by h) computed numerically and analytically as a function of the sensor angular semi-range α. The numerical results refer to three different partitions of $\mathcal{R}_d$.

ultimately they converge to the analytical results, as expected. For the sake of comparison, Fig. 6 reports dual results when the optimal landmark distance as a function of $\alpha \in (0, \pi/2)$ is normalized by h (i.e. $\frac{d^\star}{h}$ and $\frac{d^\dagger}{h}$). Notice that the trend of the curves in Figs. 5 and 6 is completely different, although numerical and analytical results are consistent. This is due to an essential geometric difference in the two cases. In Fig. 5 the SDA triangle is indeed inscribed within a circle of constant radius r. This implies that as α changes the actual sensor range h is not fixed, but it reaches a maximum for $\frac{2\pi}{9}$ and then it decreases as α approaches $\frac{\pi}{2}$. On the contrary, in Fig. 6 the SDA triangle has a constant height h, and the value of the circle radius r steadily increases with α. As a result, the normalized optimal landmark distances grow monotonically, as well. Consider that both situations may occur in real scenarios, as they depend on the setup of the sensing system (e.g. camera orientation with respect to the floor). Observe also that, in both cases, when $\mathcal{R}_d$ is partitioned into 64 sub-regions, analytical and numerical results are hardly distinguishable. For this reason, only the analytical values will be used in the rest of this paper.

TABLE I.   OPTIMAL LANDMARK DISTANCES (COMPUTED ANALYTICALLY AND NORMALIZED BY r) AND MINIMUM VALUES OF FACTOR δ FOR WHICH NO LANDMARK IS DETECTED IN AT LEAST ONE OUT OF 10^5 RANDOMLY GENERATED POSITIONS AND ORIENTATIONS OF THE SENSOR.

α [rad]	0.2	0.4	0.6	0.8	1	1.2	1.4
$\frac{d^\dagger}{r}$	0.32	0.46	0.53	0.53	0.46	0.35	0.18
δ	1.08	1.02	1.02	1.02	1.02	1.01	1.01

In order to evaluate more clearly to what extent the estimated landmark distance values are close to the optimal ones, some Monte Carlo simulations (of 10^5 runs each for given values of α) have been performed by randomly changing sensors' position and orientation over different lattices of type A^2, in which the distance between landmarks was set purposely larger than $d^\dagger$ by a variable factor δ. Tab. I reports both the optimal values of $\frac{d^\dagger}{r}$ and the minimum values of factor δ for which if we set $d = \delta \cdot d^\dagger$, there exists at least one configuration of the sensor in which no landmark is detected. It shows that for very small values of α, $d^\dagger$ is slightly far from the optimal d, e.g. approximately 8% for $\alpha = 0.2$ rad, but it tends to the optimal value when α increases.

IV.   SIMULATION RESULTS IN A CASE STUDY

In order to evaluate the impact of optimal landmark placement on localization accuracy in a real case study, the results of some Monte Carlo simulations in two different indoor environments are reported in the following, i.e. a large wide-open room without any obstacle, and a more realistic scenario based on the map of the Department of Information Engineering and Computer Science (DISI) of the University of Trento. In both environments, the trajectories are generated using the model of the *FriWalk*, the smart walker developed within the EU project ACANTO[1]. The *FriWalk* (whose dynamic can be modeled as a unicycle-like vehicle [18]) is equipped with relative encoders on the rear wheels and a front camera that measures the walker's relative position and orientation with respect to suitable visual landmarks placed on the floor. Each detected landmark (e.g. a Quick Response code) is assumed to return not only its own absolute planar coordinates (x, y) in the chosen reference frame, but also its orientation with respect to axis X_w. The main parameters of the camera's SDA (namely its field of view in the case considered) are: $r \approx 4$ m and $\alpha \approx \pi/6$ rad. Thus, it follows from (16) that $d^\dagger \approx 2$ m. The walker position is estimated by fusing odometry data and camera-based measures by means of an extended Kalman filter (EKF) [7]. The uncertainty contributions of the two encoders measuring wheels displacements at each sampling time are assumed to be uncorrelated, white and normally distributed with zero mean and variance $\sigma^2_{\Delta\phi} = 4 \cdot 10^{-4}$ rad^2. The absolute camera-based measures of position and orientation are also assumed to be affected by weakly correlated Gaussian white noises, with zero mean and variances $\sigma^2_x = 16 \cdot 10^{-4}$ m^2, $\sigma^2_y = 5 \cdot 10^{-5}$ m^2 and $\sigma^2_\theta = 10^{-3}$ rad^2, respectively [7].

A. Wide-open room case

In the ideal case of a wide-open room without obstacles where an A^2 lattice of landmarks is deployed on the floor with
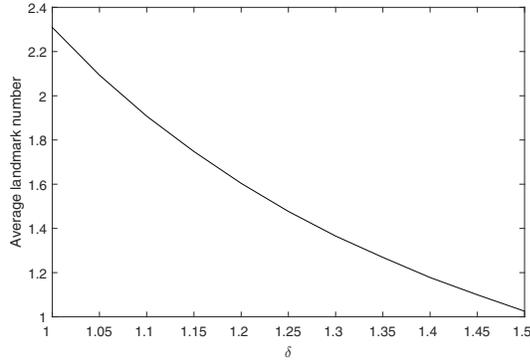

Fig. 7. Average number of detected landmarks for various adjacent landmark distances $\delta \cdot d^\dagger$ in the case of wide-open room with no obstacles.
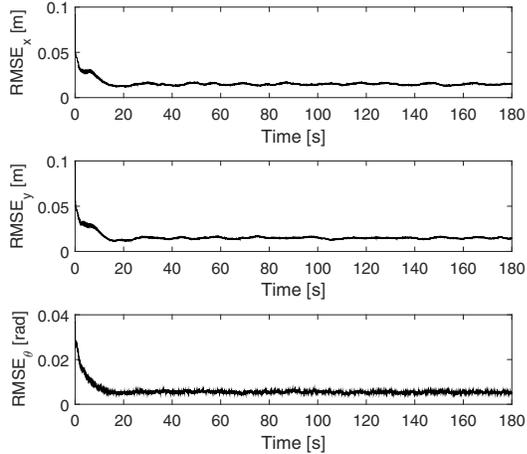

Fig. 8. RMS estimation error of robot's planar Cartesian coordinates and orientation computed over 200 random trajectories in the case of a wide-open room with no obstacles.
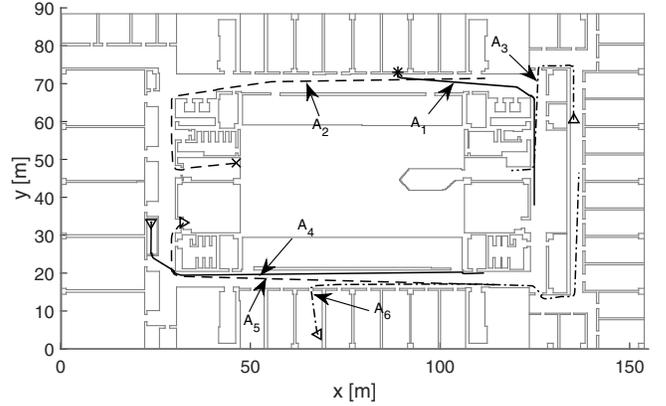

Fig. 9. Six examples of agents' trajectories in the premises of the Department of Information Engineering and Computer Science of the University of Trento.
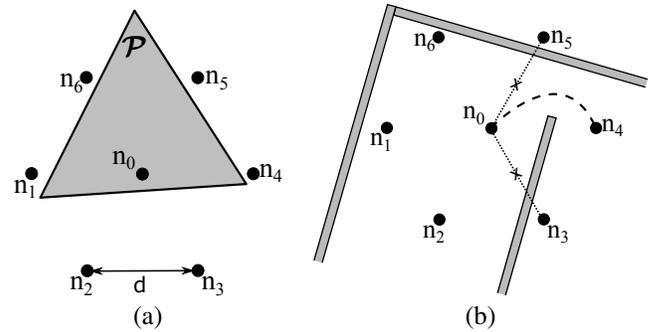

Fig. 10. Qualitative relationship between the SDA of the robot's camera, the position of a detected landmark and its six neighbors over a portion of A^2 lattice in the case of a wide-open environment (a) and a room with obstacles (e.g. walls) (b).

distances between adjacent landmarks given by (12) or (16), the front camera of the *FriWalk* is always able to detect at least one landmark, regardless of camera's position and orientation. To verify this, 200 random-walk trajectories of 180 s each have been generated within a 10×10 m wide-open room. The results obtained in this case are comparable with those reported in Tab. I. Indeed, by increasing the distance between adjacent landmarks by just a few percent with respect to the optimal value, it may happen that no landmark is detected. It is worthwhile to note that setting $d = d^\dagger$ ensures that *at least one* landmark is in view for any position and orientation of the robot. Therefore, in general, more than one landmark can be actually detected. Fig. 7 reports the average number of detected landmarks versus δ, being $\delta \cdot d^\dagger$ the parametric distance between adjacent landmarks on the lattice considered. It is evident that more than 2 landmarks can be detected on average when $d = d^\dagger$.

Fig. 8 shows the root mean square (RMS) estimation errors associated with state variables (x, y, θ) as a function of time, when 200 trajectories are simulated. Observe that all RMS error curves quickly converge to the respective lower bounds obtained using the EKF described in [7]. In fact, such lower bounds can be reached if and only if the optimal landmark deployment is adopted, i.e. if there is at least one visual landmark inside the SDA of the camera.

B. Realistic environment

The trajectories in a realistic environment (i.e. the DISI premises) have been generated using the so-called Social Force Model (SFM). This provides realistic human-like paths along with collision avoidance mechanisms [19]. Fig. 9 shows the DISI map along with six trajectories. While initial position and final destinations are generated randomly, the main difference with respect to the case of wide-open room is that now the optimal landmarks placement is affected by the presence of obstacles and walls. Anytime a point of the lattice is located inside a wall or an obstacle reported in the DISI map, obviously the corresponding landmark is not available in practice. This problem can be partially addressed by shifting all landmarks by a fixed amount until the number of those falling inside walls or obstacles is minimum. However, while in the wide-open room case, anytime the camera detects a landmark, any one of its six neighbors can be detected next [as depicted in Fig. 10(a)], the presence of walls and obstacles can make the transition from one landmark to another impossible or much less likely, e.g. because the trajectory is constrained by a wall, as shown in Fig. 10(b). This kind of situations may considerably affect RMS estimation errors even if the landmarks layout is as close as possible to the optimal one. In order to evaluate the impact of obstacles on localization accuracy, the RMS errors over time associated with the estimation of variables (x, y, θ) and

TABLE II.   AVERAGE RMS ESTIMATION ERRORS ASSOCIATED WITH VARIABLES (x, y, θ) FOR DIFFERENT VALUES OF r AND IN THE CASE OF WIDE-OPEN ROOM AND DISI PREMISES, RESPECTIVELY.

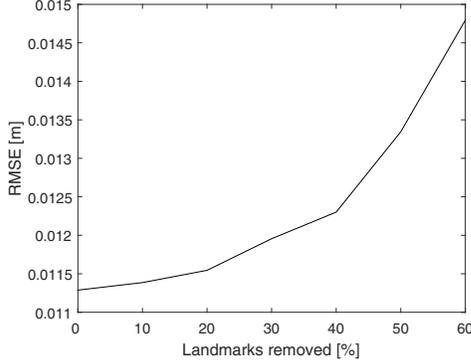|	Wide-open room			DISI premises		
r [m]	1	4	8	1	4	8
$RMSE_x$ [cm]	1.5	1.6	1.7	2.2	3.3	4.2
$RMSE_y$ [cm]	1.5	1.6	1.7	1.5	2.2	2.9
$RMSE_\theta$ [mrad]	8.0	8.0	8.0	24.0	25.0	25.0

Fig. 11.   RMS position errors between two subsequent landmark detections as a function of the percentage of landmarks randomly removed from the optimal layout.

averaged over 200 trajectories have been computed for three different values of r (i.e. 1 m, 4 m and 8 m). The corresponding results are reported in Tab. II. Observe that, in the case of wide-open room, the SDA size does not affect localization accuracy significantly, as lattice optimality for a given SDA is preserved. On the contrary, when walls and obstacles are present, the RMS position errors tend to increase as the camera SDA grows. This is due to the fact that the probability of detecting a landmark decreases from 96% when $r = 1$ m to 87% when $r = 8$ m. To emulate and to analyze the effect of the presence of obstacles more in depth, an increasing number of landmarks has been removed randomly from the optimal layout, while recomputing the RMS position errors every time. Fig. 11 shows the average RMS position error accumulated along the path between two subsequent landmarks when the percentage of removed landmarks grows. Notice that the RMS position error increases as expected, in accordance with the results reported in Tab. II.

V.   CONCLUSIONS

In this paper a landmarks optimal placement strategy for indoor localization is presented. In particular, assuming to have i) a regular triangular lattice of landmarks in a wide-open room and ii) a sensor with a limited detection area (approximated with a triangle as well), the optimal distance between pairs of adjacent landmarks is derived both numerically and analytically. Both solutions converge to the same results. The analytical solution is particularly valuable because it provides a very simple, closed-form expression, which depends just on the radial and angular detection ranges of the sensor adopted, regardless of the specific sensing technology. Therefore, it can be applied in a multitude of contexts. Also, this result could be extended to the case of square lattices of landmarks. The

results of various Monte Carlo simulations confirm that, if no obstacle is present, localization accuracy is limited mainly by the measurement uncertainty of position and orientation between the sensor and one of the landmarks. Of course, in real indoor environments, where walls and obstacles are present, an ideal optimal layout can be hardly deployed. As a consequence, just suboptimal results can be achieved, either because some landmarks could be difficult to detect or because it could impossible to place them at all. In such conditions, the longer the sensor detection range is, the higher the probability of missing some landmark becomes, thus potentially degrading localization accuracy. This issue paves the way to further research activities on placement optimization, which should take into account not only the geometry of the environment, but also the probabilities of moving from each landmark to its neighbors. In order to address this problem, a lattice of landmarks could be turned into a Markov chain model, in which nodes and edges of the resulting graph represent, respectively, the available landmarks and the transitions between pairs of them (with a given probability). The main challenge of using this model is that the transition probabilities depend on both the real paths of possible agents and the constraints imposed by the environment. So, this problem will be investigated in a future work.

APPENDIX
DERIVATION OF SYSTEM OF INEQUALITIES (7)

Let $p_{i,j} = [x_{i,j}, y_{i,j}]^T$. Since the inverse of (5) is

$$Q_\gamma^{-1} = \frac{1}{r \sin(2\beta)} \begin{bmatrix} \cos(\beta - \gamma) & -\sin(\beta - \gamma) \\ \cos(\beta + \gamma) & \sin(\beta + \gamma) \end{bmatrix},$$

the constraints on coefficients λ_1 and λ_2 can be expressed as

$$\lambda_1 \geq 0 \Leftrightarrow [1 \quad 0] \Lambda \geq 0 \Leftrightarrow [1 \quad 0] Q_\gamma^{-1} p_{i,j} \geq 0,$$
$$\lambda_2 \geq 0 \Leftrightarrow [0 \quad 1] \Lambda \geq 0 \Leftrightarrow [0 \quad 1] Q_\gamma^{-1} p_{i,j} \geq 0,$$
$$\lambda_1 + \lambda_2 \leq 1 \Leftrightarrow [1 \quad 1] \Lambda \leq 1 \Leftrightarrow [1 \quad 1] Q_\gamma^{-1} p_{i,j} \leq 1,$$

which yields to

$$\begin{cases} \cos(\beta - \gamma)x_{i,j} - \sin(\beta - \gamma)y_{i,j} \geq 0, \\ \cos(\beta + \gamma)x_{i,j} + \sin(\beta + \gamma)y_{i,j} \geq 0, \\ (\cos(\beta - \gamma) + \cos(\beta + \gamma))x_{i,j} + \\ (\sin(\beta + \gamma) - \sin(\beta - \gamma))y_{i,j} \leq r \sin(2\beta). \end{cases}$$

Hence, after some algebraic steps it follows that

$$\begin{cases} \cos(\beta - \gamma)x_{i,j} - \sin(\beta - \gamma)y_{i,j} \geq 0, \\ \cos(\beta + \gamma)x_{i,j} + \sin(\beta + \gamma)y_{i,j} \geq 0, \\ \cos(\gamma)x_{i,j} + \sin(\gamma)y_{i,j} \leq \frac{r}{2}\frac{\sin(2\beta)}{\cos(\beta)}. \end{cases} \quad (17)$$

Thus, by replacing the elements $x_{i,j}$ and $y_{i,j}$ of (4) as well as $\frac{r}{2}\frac{\sin(2\beta)}{\cos(\beta)} = r \sin(\beta) = h$ into (17), (7) finally results.

ACKNOWLEDGMENT

REFERENCES

[1] H. Liu, H. Darabi, P. Banerjee, and J. Liu, "Survey of wireless indoor positioning techniques and systems," *IEEE Trans. Syst. Man Cybern. C, Appl. Rev.*, vol. 37, no. 6, pp. 1067–1080, Nov. 2007.

[2] D. Macii, A. Colombo, P. Pivato, and D. Fontanelli, "A data fusion technique for wireless ranging performance improvement," *IEEE Trans. Instrum. Meas.*, vol. 62, no. 1, pp. 27–37, Jan. 2013.

[3] P. Nazemzadeh, D. Fontanelli, D. Macii, T. Rizano, and L. Palopoli, "Design and performance analysis of an indoor position tracking technique for smart rollators," in *Int. Conf. on Indoor Positioning and Indoor Navigation (IPIN)*, Montbeliard, France, Oct. 2013, pp. 1–10.

[4] A. A. N. Shirehjini, A. Yassine, and S. Shirmohammadi, "An rfid-based position and orientation measurement system for mobile objects in intelligent environments," *IEEE Trans. Instrum. Meas.*, vol. 61, no. 6, pp. 1664–1675, Jun. 2012.

[5] S. Holm and C. I. C. Nilsen, "Robust ultrasonic indoor positioning using transmitter arrays," in *Int. Conf. on Indoor Positioning and Indoor Navigation (IPIN)*, Zurich, Zwitzerland, Sep. 2010.

[6] R. Mautz and S. Tilch, "Survey of optical indoor positioning systems," in *Int. Conf. on Indoor Positioning and Indoor Navigation (IPIN)*, Guimaraes, Portugal, Sep. 2011, pp. 1–7.

[7] P. Nazemzadeh, F. Moro, D. Fontanelli, D. Macii, and L. Palopoli, "Indoor positioning of a robotic walking assistant for large public environments," *IEEE Trans. Instrum. Meas.*, vol. 64, no. 11, pp. 2965–2976, Nov. 2015.

[8] A. A. Khaliq, F. Pecora, and A. Saffiotti, "Inexpensive, reliable and localization-free navigation using an RFID floor," in *European Conf. on Mobile Robots (ECMR)*, Lincoln, United Kingdom, Sep. 2015, pp. 1–7.

[9] Y.-C. Wang, C.-C. Hu, and Y.-C. Tseng, "Efficient placement and dispatch of sensors in a wireless sensor network," *IEEE Trans. Mobile Comput.*, vol. 7, no. 2, pp. 262–274, Feb. 2008.

[10] Y. Chen, J.-A. Francisco, W. Trappe, and R. P. Martin, "A practical approach to landmark deployment for indoor localization," in *IEEE Conf. on Sensor, Mesh and Ad Hoc Communications and Networks (SECON)*, Reston, VA, USA, Sep. 2006.

[11] J. Zhou, J. Shi, and X. Qu, "Landmark placement for wireless localization in rectangular-shaped industrial facilities," *IEEE Trans. Veh. Technol.*, vol. 59, no. 6, pp. 3081–3090, Jul. 2010.

[12] M. Beinhofer, J. Müller, and W. Burgard, "Effective landmark placement for accurate and reliable mobile robot navigation," *ROBOT. AUTON. SYST.*, vol. 61, no. 10, pp. 1060–1069, Oct. 2013.

[13] M. Beinhofer, J. Mller, A. Krause, and W. Burgard, "Robust landmark selection for mobile robot navigation," in *2013 IEEE/RSJ International Conference on Intelligent Robots and Systems*, Nov 2013, pp. 3637–2643.

[14] P. Sala, R. Sim, A. Shokoufandeh, and S. Dickinson, "Landmark selection for vision-based navigation," *IEEE Trans. Robot.*, vol. 22, no. 2, pp. 334–349, Apr. 2006.

[15] L. H. Erickson and S. M. LaValle, "An art gallery approach to ensuring that landmarks are distinguishable," in *Robotics:Science and Systems*, Los Angeles, CA, USA, Jun. 2011.

[16] W. W. R. Ball, *Mathematical recreations and essays*. MacMillan, 1914.

[17] C. D. Toth, J. O'Rourke, and J. E. Goodman, *Handbook of discrete and computational geometry*. CRC press, 2004.

[18] L. Palopoli, A. Argyros, J. Birchbauer, A. Colombo, D. Fontanelli, A. Legay, A. Garulli, A. Giannitrapani, D. Macii, F. Moro, P. Nazemzadeh, P. Padeleris, R. Passerone, G. Poier, D. Prattichizzo, T. Rizano, L. Rizzon, S. Scheggi, and S. Sedwards, "Navigation Assistance and Guidance of Older Adults across Complex Public Spaces: the DALi Approach," *Intelligent Service Robotics*, vol. 8, no. 2, pp. 77–92, 2015.

[19] D. Helbing and P. Molnár, "Social force model for pedestrian dynamics," *Phys. Rev. E Stat. Nonlin. Soft.*, vol. 51, pp. 4282–4286, May 1995.